WHITE PAPER

Multispectral Fingerprint Image Acquisition

Robert K. Rowe, Kristin Adair Nixon, Paul W. Butler

Published in *Advances in Biometrics*, Springer, 2008
Editors N.K. Ratha and V. Govindaraju

Abstract

This chapter describes the principles of operation of a new class of fingerprint sensor based on multispectral imaging (MSI). The MSI sensor captures multiple images of the finger under different illumination conditions that include different wavelengths, different illumination orientations, and different polarization conditions. The resulting data contain information about both the surface and subsurface features of the skin. This data can be processed to generate a single composite fingerprint image equivalent to that produced by a conventional fingerprint reader, but with improved performance characteristics. In particular, the MSI imaging sensor is able to collect usable biometric images in conditions where other conventional sensors fail such as when topical contaminants, moisture, and bright ambient lights are present or there is poor contact between the finger and sensor. Further, the MSI data can be processed to ensure that the measured optical characteristics match those of living human skin, providing a strong means to protect against attempts to spoof the sensor.

Introduction

Biometric systems are deployed in order to provide a means of fixing the identity of individuals in an automated manner. In order for such a deployment to be successful, the biometric sensor needs to be able to collect useful data over the entire range of conditions in which it operates. These conditions include differences between users as well as variations in the environment in which the biometric measurement is taken. In addition, a biometric system should also be able to detect attempts to defeat it using some type of artificial sample without compromising successful use by a genuine authorized person. All of these capabilities should be able to be performed quickly and without extra steps or inconveniences to the authorized user.

Fingerprint sensing is one of the most widely deployed of all biometric technologies. There are a number of different techniques for capturing a fingerprint image including optical, capacitive, radio frequency, ultrasound, and thermal methods. One common shortcoming of many conventional fingerprint sensing technologies is the frequent occurrence of poor-quality images under a variety of common operational circumstances. Though each particular imaging method has different sensitivities, in general poor images may result from conditions such as dry skin, worn surface features of the finger, poor contact between the finger and sensor, bright ambient light, and moisture on the sensor.

Many imaging technologies are also unable to provide strong affirmation that the fingerprint image is collected from a living, unadulterated finger rather than an artificial or spoof sample. This is so because the raw data collected by these systems contain little or no information about the physical properties of the fingerprint ridges presented. For example, a conventional optical fingerprint reader based on total internal reflectance (TIR) acquires images that represent the points of optical contact between the sensor platen and any material with a minimum index of refraction. Because many

materials have an appropriate refractive index and can be formed to contain a fingerprint pattern, such a system is susceptible to spoof attempts.

To address these shortcomings, an optical fingerprint sensor has been developed that is able to work across the range of common operational conditions while also providing strong spoof detection. The sensor is based on multispectral imaging (MSI) and is configured to image both the surface and subsurface characteristics of the finger under a variety of optical conditions. The combination of surface and subsurface imaging ensures that usable biometric data can be taken across a wide range of environmental and physiological conditions. Bright ambient lighting, wetness, poor contact between the finger and sensor, dry skin, and various topical contaminants present little impediment to collecting usable MSI data.

A customized algorithm is used to fuse multiple raw MSI images into a single high-quality composite fingerprint image. This single fingerprint image can be used to match other MSI fingerprint images as well as images collected using other methods. Thus, the MSI fingerprint is backward compatible and can be used with existing fingerprint databases collected with different imaging technologies.

The surface and subsurface data collected by the MSI sensor provide rich information about the optical properties of the bulk sample. A classification methodology has been developed to operate on the MSI data and determine if the measured optical properties of the sample are consistent with those of living human skin. If so, the sample is deemed to be genuine; otherwise, the sample is identified as a possible spoof attempt. This provides the means by which an MSI sensor can provide strong assurance of sample authenticity.

This chapter describes the principles of operation of an MSI fingerprint sensor and illustrates the type of raw data that is collected. The methods used for generating a composite fingerprint are described and examples given. Medium-scale biometric performance testing procedures and results using these composite fingerprint images are provided. In a later section of this chapter, procedures and results from a study conducted under a variety of adverse conditions will be presented. This study includes both an MSI fingerprint sensor as well as three common commercially available optical fingerprint sensors. Data from the same study is also analyzed in a way that demonstrates the cross-compatibility of MSI fingerprint images with those collected from conventional imagers. The final section of this chapter discusses MSI spoof detection methods and quantifies spoof detection performance.

Finger Skin Histology

Human skin is a complex organ that forms the interface between the person and the outside environment. The skin contains receptors for the nervous system, blood vessels to nourish the cells, sweat glands to aid thermal regulation, sebaceous glands for oil secretion, hair follicles, and many other physiologically important elements. As well, the skin itself is not a single, homogeneous layer, but is made of different layers with different material properties. These different layers can be broadly separated into the epidermis, which is the most superficial layer, the dermis, which is the blood-bearing layer, and the subcutaneous skin layer which contains fat and other relatively inert components.

The skin on the palmar side of the finger tips contains dermatoglyphic patterns comprising the ridges and valleys commonly measured for fingerprint-based biometrics. Importantly, these patterns do not exist solely on the surface of the skin—many of the anatomical structures below the surface of the skin mimic the surface patterns. For example, the interface between the epidermal and dermal layers of skin is an undulating layer made of multiple protrusions of the dermis into the epidermis known as dermal papillae. These papillae follow the shape of the surface dermatoglyphic patterns (Cummins and Midlo 1961) and thus represent an internal fingerprint in the same form as the external pattern. Small blood vessels known as capillaries protrude into the dermal papillae

(Sangiorgi 2004) as shown in Fig. 1. These blood vessels form another representation of the external fingerprint pattern.

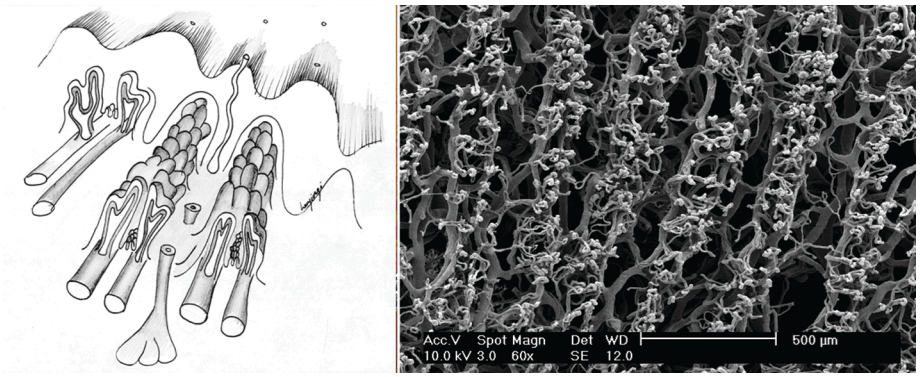

Fig. 1. Histology of the skin on the palmar surface of the fingertip. The sketch on the left shows the pattern of the capillary tufts and dermal papillae that lie below the fingerprint ridges. The SEM photo on the right side shows the rows of capillary tufts imaged on a portion of an excised thumb after the surrounding skin has been removed (Simone Sangiorgi, personal communication, 2005).

There are various methods that can be used to image the internal structure of the skin of the finger. One method is the use of optics. Recently published research demonstrated the use of optical coherence tomography to investigate features of the finger skin below the ridges and valleys (Shirastsuki 2005). This research showed that there was a distinct area of high reflectivity (at 850 nm) in the skin approximately 500 µm below each finger ridge. Furthermore, the researchers were able to demonstrate that this subsurface pattern continued to exist even when the surface pattern was deformed by application of high pressure or obscured by a wrinkle in the skin.

Multispectral imaging represents another optical method that can be used to capture surface and subsurface features of the skin. The remainder of this chapter will provide details on MSI operational principles as well as tests and results from this type of fingerprint sensor.

MSI Principles of Operation

In order to capture information-rich data about the surface and subsurface features of the skin of the finger, the MSI sensor collects multiple images of the finger under a variety of optical conditions. The raw images are captured using different wavelengths of illumination light, different polarization conditions, and different illumination orientations. In this manner, each of the raw images contains somewhat different and complementary information about the finger. The different wavelengths penetrate the skin to different depths and are absorbed and scattered differently by various chemical components and structures in the skin. The different polarization conditions change the degree of contribution of surface and subsurface features to the raw image. Finally, different illumination orientations change the location and degree to which surface features are accentuated.

Figure 2 shows a simplified schematic of the major optical components of an MSI fingerprint sensor. Illumination for each of the multiple raw images is generated by one of the light emitting diodes (LEDs). The figure illustrates the case of polarized, direct illumination being used to collect a raw image. The light from the LED passes through a linear polarizer before illuminating the finger as it rests on the sensor platen. Light interacts with the finger and a portion of the light is directed toward the imager through the imaging polarizer. The imaging polarizer is oriented with its optical axis to be orthogonal to the axis of the illumination polarizer, such that light with the same polarization as the illumination light is substantially attenuated by the polarizer. This severely reduces the influence of

light reflected from the surface of the skin and emphasizes light that has undergone multiple optical scattering events after penetrating the skin.

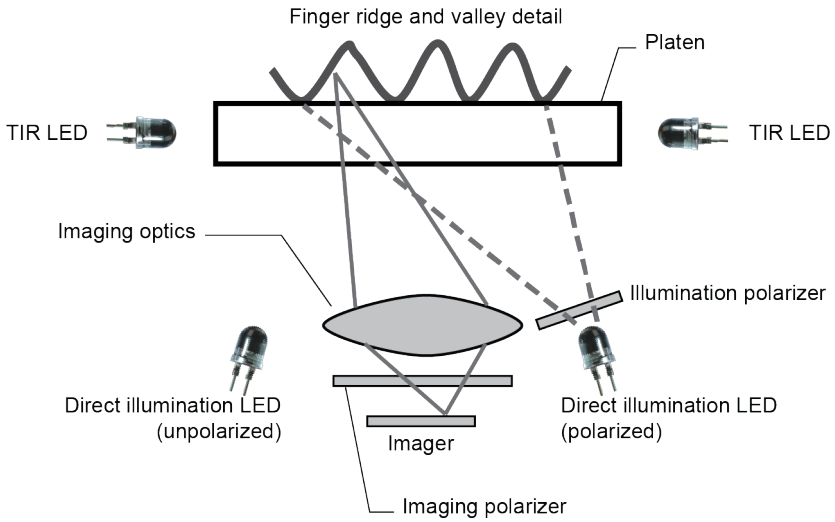

Fig. 2. Optical configuration of an MSI sensor. The dotted lines illustrate the direct illumination of a finger by a polarized LED.

The second direct illumination LED shown in Fig. 2 does not have a polarizer placed in the illumination path. When this LED is illuminated, the illumination light is randomly polarized. In this case the surface-reflected light and the deeply penetrating light are both able to pass through the imaging polarizer in equal proportions. As such, the image produced from this non-polarized LED contains a much stronger influence from surface features of the finger.

Importantly, all of these direct illumination sources (both polarized and non-polarized) as well as the imaging system are arranged to avoid any critical-angle phenomena at the platen-air interfaces. In this way, each illuminator is certain to illuminate the finger and the imager is certain to image the finger regardless of whether the skin is dry, dirty or even in contact with the sensor. This aspect of the MSI imager is distinctly different from most other conventional fingerprint imaging technologies and is a key aspect of the robustness of the MSI methodology.

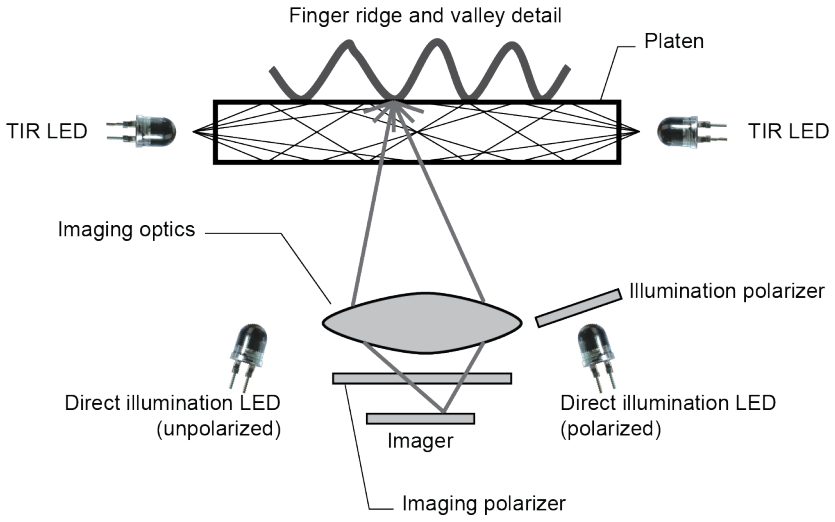

Fig. 3. MSI sensor schematic showing TIR illumination.

In addition to the direct illumination illustrated in Fig. 2, the MSI sensor also integrates a form of TIR imaging, illustrated in Fig. 3. In this illumination mode, one or more LEDs illuminate the side of the platen. A portion of the illumination light propagates through the platen by making multiple TIR reflections at the platen-air interfaces. At points where the TIR is broken by contact with the skin, light enters the skin and is diffusely reflected. A portion of this diffusely reflected light is directed toward the imaging system and passes through the imaging polarizer (since this light is randomly polarized), forming an image for this illumination state. Unlike all of the direct illumination states, the quality of the resulting raw TIR image is critically dependent on having skin of sufficient moisture content and cleanliness making good optical contact with the platen, just as is the case with conventional TIR sensors. However, unlike conventional TIR sensors, the MSI sensor is able to form a useable representation of the fingerprint from the direct illumination images even when the TIR image is degraded or missing. Further details of this will be provided in later sections of this chapter.

In practice, MSI sensors typically contain multiple direct-illumination LEDs of different wavelengths. For example, the Lumidigm J110 MSI sensor is an industrial-grade sensor that has four direct-illumination wavelength bands (430, 530, and 630 nm as well as a white light) in both polarized and unpolarized configurations. When a finger is placed on the sensor platen, eight direct-illumination images are captured along with a single TIR image. The raw images are captured on a 640 x 480 image array with a pixel resolution of 525 ppi. All nine images are captured in approximately 500 mSec.

In addition to the optical system, the Lumidigm J110 comprises control electronics for the imager and illumination components, an embedded processor, memory, power conversion electronics, and interface circuitry. The embedded processor performs the image-capture sequence and communicates to the rest of the biometric system through the interface circuitry. In addition to controlling the image acquisition process and communications, the embedded processor is capable of processing the nine raw images to generate a single 8-bit composite fingerprint image from the raw data. The embedded processor also analyzes the raw MSI data to ensure that the sample being imaged is a genuine human finger rather than an artificial or spoof material. Composite fingerprint image generation and spoof detection will be described in greater detail in the following sections. In some applications, the J110 is also configured to perform on-board feature extraction and matching.

Composite Fingerprint Image Generation

As described in the previous section, multiple raw images of the finger are collected each time a finger touches the sensor. These multiple images correspond to different illumination wavelengths, polarization conditions, and optical geometries. As such, each contains a slightly different representation of the characteristics of the finger, including the fingerprint itself. An example of the raw images derived during a single measurement from a Lumidigm J110 MSI sensor is shown in Fig. 4. The upper row shows the raw images for unpolarized illumination wavelengths of 430, 530, and 630 nm, as well as white light. The middle row shows the corresponding images for the cross-polarized case. The single image on the bottom row is the TIR image. The grayscale for each of the raw images has been expanded to emphasize the features.

It can be seen from the figure that there are a number of features present in the raw data including the textural characteristics of the subsurface skin, which appears as mottling that is particularly pronounced under blue (430 nm) and green (530 nm) illumination wavelengths. As well, the relative intensities of the raw images under each of the illumination conditions is very indicative of the spectral characteristics (i.e. color) of the finger or other sample (note that the relative intensities have been obscured in Fig. 4 to better show the comparative details of the raw images). Both textural and spectral characteristics play a key role in spoof detection since each exhibits distinct

differences between living skin and most other materials. Methods of using these characteristics for spoof detection will be more fully described in a later portion of this chapter.

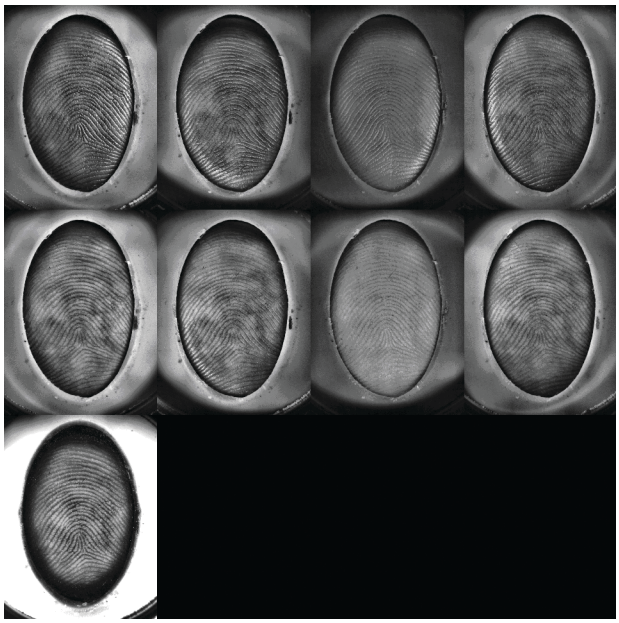

Fig. 4. Raw MSI images. The upper row of images corresponded to cross-polarized illumination of various wavelengths, the middle row corresponds to cross-polarized illumination, and the bottom left image is a backscattered image.

Also of note in the raw images is the area of the finger that each captures. The directly illuminated images in the top and middle rows capture details over nearly the entire surface of the finger. In contrast, the TIR image in the bottom row only captures features from a smaller, central portion of the finger, as evinced by the size of the illuminated region in the image. This difference is due to the fact that the TIR image requires optical contact between the finger and platen to generate an image while the direct illumination does not require contact and can thus effectively capture features of the finger even in those areas where there is a gap between the skin and the platen. This is significant because the MSI images contain information about the finger over a bigger area than an equivalent surface-based imaging technology is capable of capturing, which would be expected to result in additional biometric features (e.g. minutiae) and a corresponding improvement in biometric performance.

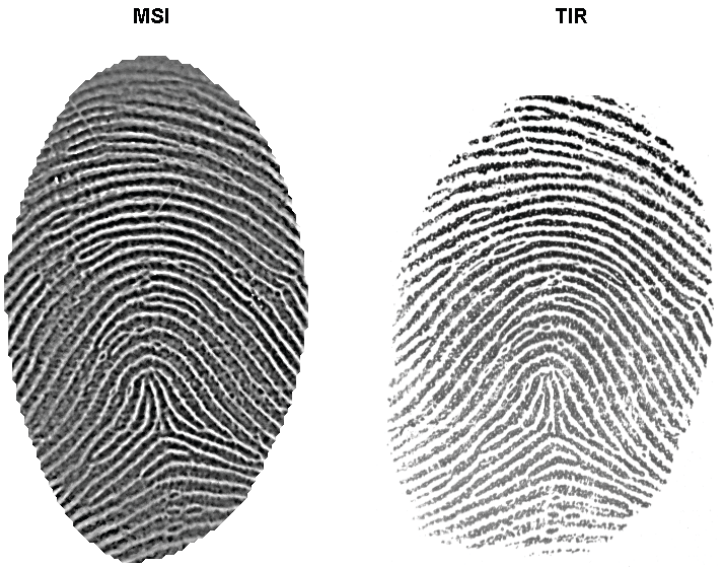

Fig. 5. On the left is a composite fingerprint image generated from the raw MSI images shown in Fig. 4. On the right is a conventional TIR image collected on the same finger used to generate the MSI fingerprint.

The set of raw images shown in Fig. 4 can be combined together to produce a single representation of the fingerprint pattern. This fingerprint generation relies on a wavelet-based method of image fusion to extract, combine, and enhance those features that are characteristic of a fingerprint. The wavelet decomposition method that is used is based on the dual-tree complex wavelet transform (Kingsbury, 2001). Image fusion occurs by selecting the coefficients with the maximum absolute magnitude in the image at each position and decomposition level (Hill, et al., 2002). An inverse wavelet transform is then performed on the resulting collection of coefficients, yielding a single, composite image. An example of the result of applying the compositing algorithm to the raw data in Fig. 4 is shown in Fig. 5. Fine structure such as incipient fingerprint ridges can be seen throughout the image. For comparison, a conventional (TIR) fingerprint image was collected on the same finger and is also shown.

Biometric Testing and Results

Baseline Performance

The baseline performance of the J110 MSI sensor was assessed in a recent multi-person study. Three Lumidigm J110 sensors were deployed in the study in which 118 people were recruited to participate. The study duration was three weeks long, during which time the volunteers made multiple visits. Volunteers were divided roughly evenly between males and females. The ages ranged between 18 and over 80 years old. Volunteers were not prescreened for any particular characteristic and the demographic distribution of the volunteers participating in the study generally reflected the local (Albuquerque, New Mexico) population.

All fingers (i.e. index, middle, ring, and little finger) of the right hand of each volunteer were measured at multiple times throughout the study. The first three presentations of a particular finger on the first J110 sensor were used as enrollment data against which data taken on all other sensors and during subsequent visits were compared. Volunteers came “as they were” to each study session and were not asked to wash their hands or pretreat the finger skin in any way.

The biometric performance was assessed using a feature extraction and matching algorithm supplied by NEC (NECSAM FE4, ver. 1.0.2.0, PPC2003). The match values were generated by comparing each of the verification templates against each of the three enrollment templates and the

highest match value was taken. All properly labeled images were used for the analysis of biometric performances. The only images that were omitted from analysis were a small number that were collected on incorrect fingers. These occurrences were assessed using web cameras and other supplemental means and were not based on the fingerprint match itself.

The receiver operating characteristic (ROC) curve generated from the study is shown in Fig. 6. The equal error rate (EER) is approximately 0.8% and the false rejection rate (FRR) at a false acceptance rate (FAR) of 0.01% is approximately 2.5%, corresponding to a true acceptance rate (TAR) of 97.5%. The total number of true-match comparisons used for this curve is 5,811 and the number of false-match comparisons is 58,110, randomly chosen from all possible false-match comparisons.

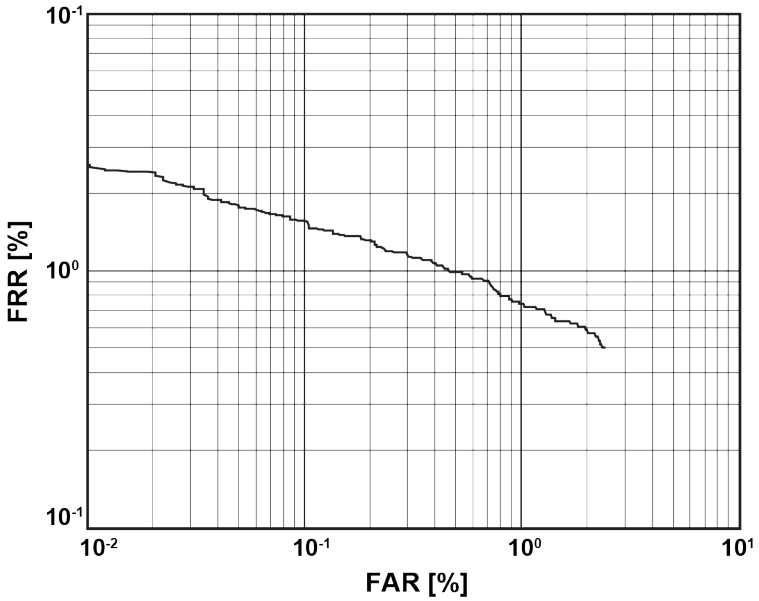

Fig. 6. Baseline biometric performance of the J110 MSI fingerprint sensor assessed during a three-week study of 118 volunteers using all four fingers (index, middle, ring, and little finger) of their right hand.

Comparative Performance under Adverse Influences

The hypothesis that the MSI sensor has the ability to collect usable biometric data under conditions where the performance of other sensors degrades or the sensor stops working was tested in a series of comparative multi-person studies. The studies included both an MSI sensor as well as several conventional TIR fingerprint sensors. In order to draw a strong conclusion from the study and avoid spurious results, key aspects of the experiment were varied and the resulting findings were compiled together to yield the overall conclusions. These key experimental aspects include:

- Conventional TIR sensor performance was assessed using three different commercially available TIR sensors from three different manufacturers.
- Three different commercially available feature extractors and matchers were used to assess biometric performance across all images.
- Six different adverse conditions were tested.

In addition to the Lumidigm J110 MSI fingerprint sensor, the three conventional TIR sensors used in the study were:

- Cross Match Verifier 300 (“Sensor C”)
- Identix DFR 2100 (“Sensor I”)

- Sagem Morpho MSO 300 (“Sensor S”)

The three commercially available fingerprint algorithms used to generate results from all images were from NEC, Sagem, and Neurotechnologija. The results presented below were generated by taking the average of the results produced by each of these algorithms.

The six different adverse conditions that were tested were as follows:

- Acetone: Approximately a teaspoon of acetone was poured on each finger and allowed to dry prior to the collection of each image.
- Chalk: The volunteer was asked to take a small pinch of chalk and rub it between his/her fingers prior to each image collection. The chalk was white climber’s chalk obtained from a local sporting goods store.
- Dirt: The volunteer was asked to take a small pinch of dirt and rub it between his/her fingers prior to image collection. The dirt was collected locally and consisted of sand, small stones, humus, etc.
- Water: The volunteer was asked to dip their finger in a glass of water and immediately place the wet finger on the sensor prior to each image collection.
- Low pressure: The volunteer was asked to “barely touch” the sensor, resulting in an estimated force of 0.2–3.0 ounces.
- Bright ambient light: Three quartz tungsten halogen (QTH) lamps with a total wattage of 1100 W were placed at a height of approximately 30” and a fixed orientation relative to the platen of each sensor. This resulted in an incident intensity of approximately 7.35 K Lux on the platen surface when no finger was present.

The study of the effect of these adverse conditions was initiated by recruiting approximately 20 volunteers for each experimental session (not all volunteers were able to participate in all portions of the study) from the local office environment. Each volunteer enrolled four fingers (left middle, left index, right index, right middle) on each of the study sensors under benign indoor ambient conditions. Enrollment consisted of collecting three high-quality images of each finger during a supervised session. During the enrollment session, the expert supervisor examined each image prior to accepting it in order to ensure that the image was properly centered and contained good detail about the fingerprint pattern. In some cases a volunteer was asked to place a small amount of skin lotion on their fingertips in order to obtain an image of sufficient quality from one or more of the conventional TIR sensors.

On subsequent test days, the volunteers presented themselves at the measurement station and images would be taken of each of the enrolled fingers under the designated adverse condition for the session. All of the sensors were tested during each session, in close succession, and under as similar conditions as possible. In some cases, one or more of the conventional TIR sensors experienced a failure to acquire (FTA) due to the real-time image acquisition logic incorporated in the sensor. In those cases where a volunteer was unable to successfully collect an image after approximately ten seconds, a blank image was inserted in its place and used in the subsequent analysis.

Each of the images in the resulting datasets was matched against each of the enrollment images. The highest match value across the three enrollment images was saved and accumulated to compile the matching and non-matching values and resulting performance curves for each of the three feature-extraction and matching packages. The final results were generated by averaging together the performance values for the three matchers.

The size of the dataset for each adverse condition was approximately 230 images, which was used to generate an equivalent number of true-match comparison values. The number of false-match comparisons used for each condition and algorithm varied between 5,676 and 22,700 randomly selected from all possible false-match comparisons.

A table summarizing the resulting average biometric performance of each of the tested sensors under each adverse condition is given in Table 1. The table shows the TAR corresponding to an FAR=0.01%.

	Sensor C	Sensor I	Sensor S	MSI Sensor
Acetone	62.9	97.0	82.8	99.1
Chalk	0.1	1.9	2.2	91.8
Dirt	0.5	7.8	4.3	85.9
Water	18.4	12.1	14.4	99.3
Low pressure	40.2	52.9	39.5	98.0
Bright ambient	5.5	48.8	99.3	99.8
Average (all conditions)	21.3	36.8	40.4	95.7

Table 1. TAR (%) at an FAR of 0.01%. Sensor C is a Cross Match Verifier 300, Sensor I is an Identix DFR 2100, Sensor S is a Sagem MSO300, and the MSI Sensor is a Lumidigm J110.

The performance of the MSI sensor can be seen to be significantly better than the conventional sensors in both the average case and in most specific instances. In some cases, the performance difference is quite dramatic (e.g. the case of water on the platen). This performance difference is generally maintained at all operating points along the respective ROC curves.

Backward Compatibility with Legacy Data

The enrollment and verification data collected with the four different sensors and the six different adverse conditions was analyzed a second way to assess the ability of the MSI images to be matched to images collected from conventional TIR fingerprint sensors. To make this assessment, the MSI images that were collected under the adverse conditions were matched to the enrollment data collected from each of the conventional TIR sensors. As before, the analysis was repeated for each of the three extractor-matcher software packages. Table 2 summarizes the resulting average performance results.

	Enroll Sensor C		Enroll Sensor I		Enroll Sensor S	
	Verify Sensor C	Verify MSI	Verify Sensor I	Verify MSI	Verify Sensor S	Verify MSI
Acetone	62.9	99.8	97.0	100	82.8	100
Chalk	0.1	95.8	1.9	97.1	2.2	95.0
Dirt	0.5	89.3	7.8	95.9	4.3	88.0
Water	18.4	99.5	12.1	98.0	14.4	99.2
Low pressure	40.2	99.3	52.9	99.3	39.5	99.3
Bright ambient	5.5	99.7	48.8	99.7	99.3	99.1
Average (all conditions)	21.3	97.2	36.8	98.3	40.4	96.8

Table 2. TAR (at FAR=0.01%) for same-sensor and cross-sensor cases. The same-sensor performance (shaded) duplicates the information in Table 1. The corresponding cross-sensor performance is generated using enrollment data collected with Sensors C, I, S and performing biometric comparisons to MSI images collected under adverse conditions.

The non-shaded columns of data represent the cross-sensor matching results, while the shaded columns are the corresponding same-sensor match results repeated from Table 1. A comparison of the cross-sensor and same-sensor results shows a dramatic improvement in nearly every tested instance as well as the overall average. This finding indicates that the MSI imaging technology is

compatible with legacy data collected on conventional TIR fingerprint sensors. Moreover, the performance improvements of the MSI sensor operating in adverse conditions can be realized even in cases where the enrollment data are taken under a different imaging method. This is consistent with the premise that an MSI imager can acquire raw data sufficient to produce a high-quality composite fingerprint image under conditions where other technologies experience severe performance degradation.

Spoof Detection

A successful biometric system must be able to reliably identify live, human fingerprints and reject all others. Spoof detection, also called liveness detection, is the ability to distinguish a fingerprint generated from a live human finger from one generated by any other material. Recently, numerous articles have been published demonstrating various methods of spoofing conventional fingerprint technologies. Methods range from the very simple, such as breathing on a sensor to reactivate a latent print (Thalheim, Krissler, and Ziegle 2002), to the more sinister method of using a cadaver finger (Parthasaradhi 2003). The more common method of spoofing a fingerprint reader is to create a replica of a fingerprint using easily available materials such as clear tape and graphite powder (Thalheim, Krissler, and Ziegle 2002), Play-Doh or latex (Derakhshani 1999), silicone or gelatin (Matsumoto, Matsumoto, Yamada, and Hoshino 2002), a rubber stamp (Geradts and Sommer 2006), or clay (Parthasaradhi 2003).

Conventional fingerprint sensors collect images based on the difference between air and material in contact with the sensor. While each sensor technology differs in its capture method, each relies on only a single property of the material in contact with the sensor. Optical fingerprint sensors use the difference in the refractive index, solid state sensors rely on the difference in impedance, and thermal sensors rely on the difference in thermal conductivity. Any material placed on a sensor that has the same property as expected can be used to capture a fingerprint. For example, an optical fingerprint reader will collect an image from a three-dimensional fingerprint made of any appropriate material that contacts the sensor, such as latex, silicone, or gelatin. The weakness of conventional readers is their reliance on a single property of the surface of the material containing the fingerprint. Once any material that replicates the surface property is discovered, it can be used to consistently spoof the sensor. A more reliable method of spoof detection would allow multiple properties of the both the surface and the subsurface of the skin to be measured.

The multiple color images acquired at different polarizations and angles allow a MSI sensor to capture many properties of the finger useful for spoof detection. In general, the properties of a material captured in MSI data may be broken down into two broad categories: spectral and spatial/textural. The simplest spectral property is that of the color of the surface of the material placed on the sensor. The range of live human skin colors is fairly narrow and, visually, skin on its surface looks very different from many other materials. This property is very easily seen through the intensity of the pixels in each of the MSI image planes. An illustration of the ability to use average spectral properties as a discriminant is given in Fig. 7. The four plots show the mean image intensity value for four different types of spoofs (red gelatin, gold latex, white clay, and green gummy bear material, each formed into fingerprint patterns) measured over a representative set of samples. In each of the plots, the average intensity value for a representative population of volunteers is repeated. The spoofs are shown as dotted lines and the average human values are shown as solid lines. Also plotted for all curves are the error bounds that describe the +/- 3 standard deviation variation of the particular average intensity value for the given sample class. It can be seen that in many image planes, the separation of the average intensity values are highly significant, implying easy class separation based only on this single, rudimentary parameter.

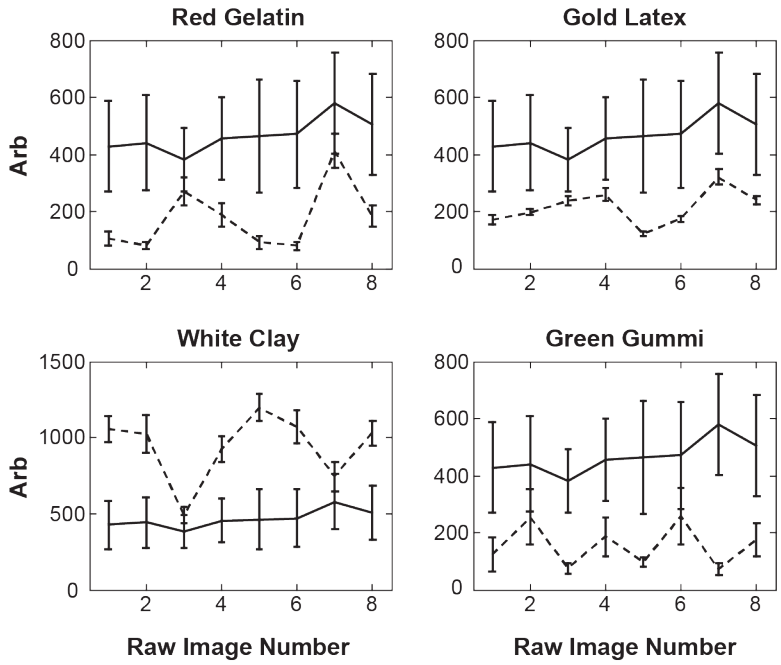

Fig. 7. Spectral differences between people and various spoof types. The average image intensity for each of the eight direct-illumination images is plotted for people (solid lines, repeated in the four plots) and spoofs (dotted lines, different for each plot). Error bounds represent 3*STD of the measured population for each sample class. All of these sample types are clearly separable from people based only their average spectral properties.

More complex properties are also captured in the MSI data. For example, different colors of light interact with different properties of skin and components of skin such as blood. Work in medical spectroscopy demonstrates how the major components of blood (oxygenated and deoxygenated hemoglobin) absorb at different wavelengths of light, as shown in Fig. 8. Oxygenated hemoglobin is highly absorbing at wavelengths above 600 nm. Below 600 nm, both forms of hemoglobin become highly absorbing, but with distinctly different spectral properties. The different illumination wavelengths of the MSI sensor effectively perform a coarse measurement of the spectrum of the skin of which the spectrum of blood should be a major component. By properly interrogating the MSI data, the presence or absence of blood in the sample may be determined, providing another strong means to discriminate against certain types of spoof samples.

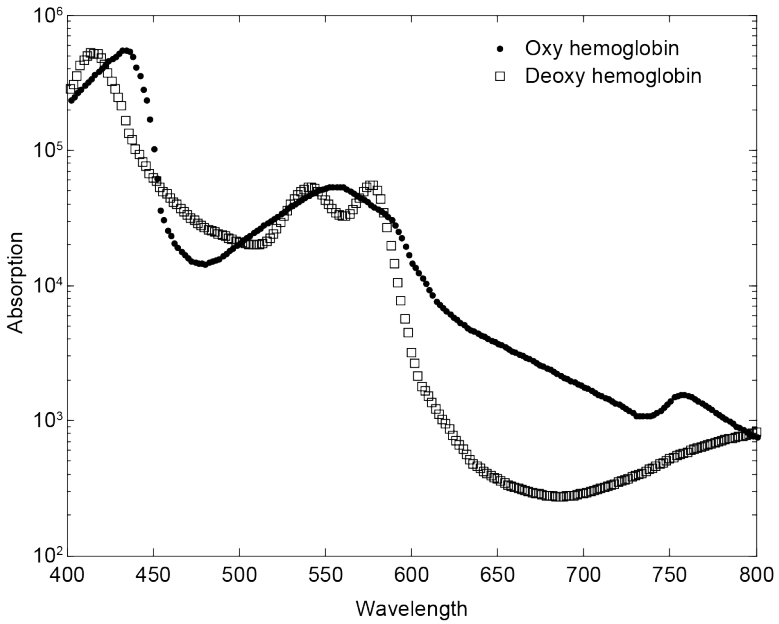

Fig. 8. Comparison of spectra of oxygenated and deoxygenated hemoglobin

Spatial and textural characteristics are also extremely important for spoof detection. For example, when certain thin and transparent materials are placed over the finger in an attempt to spoof the system, fingerprint patterns from both the thin sample as well as the underlying finger may be observed. This composite of fingerprint features often results in unnatural textures such as cross-hatching, as illustrated by several examples in Fig. 9. Classification methods are readily able to discriminate between normal and abnormal textures and thus provide another avenue for detecting attempts to spoof the sensor.

Because of the large variety and possibilities in authentic fingerprint features, the problem of effectively selecting and combining features to differentiate spoofs is unique to the MSI technology. One way to select and create conglomerate features is through multivariate data-driven learning techniques, such as neural networks or discriminate analysis (Duda, Hart, and Stork 2001). These methods use examples to determine the features and their combination that are most useful to distinguish between classes: in this case, classes of live, human fingerprints and all other materials. In addition to being robust against a variety of spoofs, this also gives the distinct advantage of being able to adapt to new spoofs as they are discovered.

To rigorously test the spoof detection abilities of the multispectral system, a study was conducted using a representative population of human volunteers and a large assortment of spoof samples. The volunteers were the same 118 people described earlier as having made multiple visits over a three-week period. Spoof samples comprised all spoof types described in the open literature as well as some additional sample types. A total of 49 types of spoofs were collected. Latex, silicone, Play-Doh, clay, rubber, glue, resin, gelatin, and tape were used in various colors, concentrations, and thicknesses. Multiple prosthetic fingers were also used. Each of the transparent and semitransparent spoof samples were tested in conjunction with each of the volunteers' index fingers. The spoof sample was placed on top of the volunteer's finger prior to touching the sensor and collecting the MSI data. A total of 17,454 images were taken on the volunteers' real fingers and 27,486 spoof images were collected. For each class of spoof, between 40 and 1940 samples were collected. Transparent spoofs worn by the volunteers' index fingers resulted in an order of magnitude more samples than opaque spoofs.

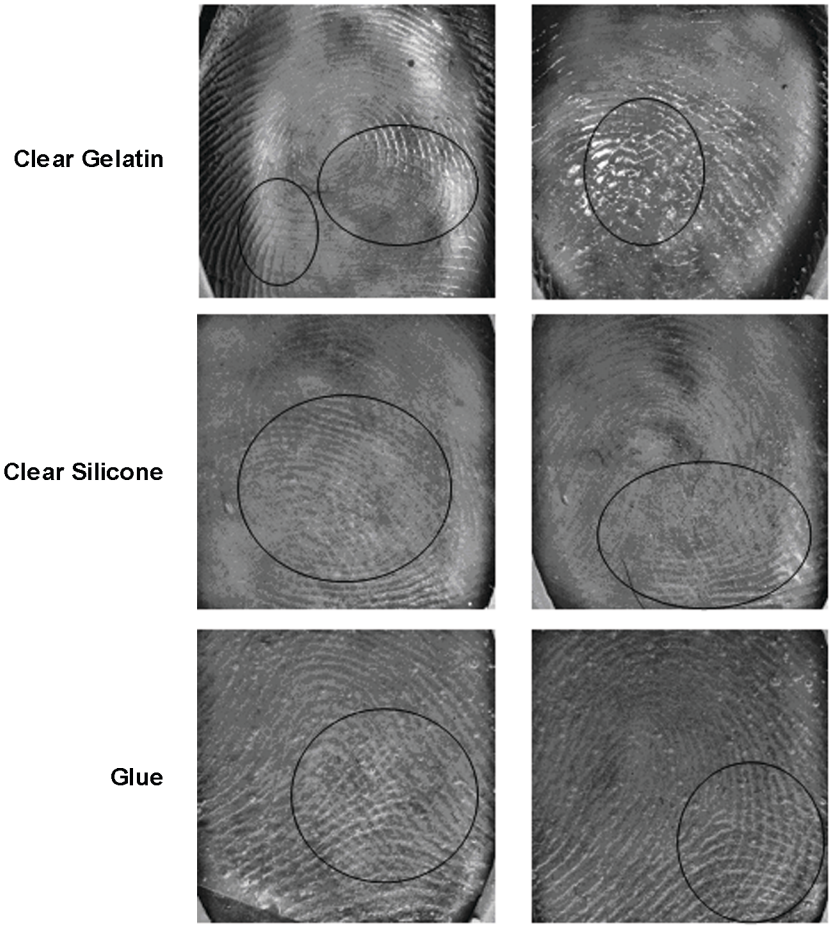

Fig. 9. Example images of various thin, transparent spoofs placed on real fingers. The elliptical marks highlight areas in which unnatural textures are clearly apparent. The automated texture analysis techniques incorporated in the MSI sensor are sensitive to much subtler variations of texture.

Each MSI image stack underwent a wavelet transform using dual-tree complex wavelets (Kingsbury, 2001). The absolute magnitudes of the coefficients were then summed over all six decomposition orientations. The resulting summed coefficient values were compiled into histograms for each raw MSI image and each decomposition level. Each of the resulting histograms were then summarized at two percentile values (30th and 70th). The compilation of all the summary values for all levels and all raw images then formed a vector of independent variables used to classify a particular sample as genuine or spoof. A variant of Fisher's linear discriminant was applied to a training set of data and was used to create eight features for classification. For testing, the difference between the squared Euclidian distance to the spoof and person class means was used to calculate the error trade-off of correctly classifying a subject and misclassifying a spoof. The results are shown in Fig. 10, which is similar to the ROC curves used to describe biometric matching performance over a range of operating points. In this case, the TAR is the rate at which a measurement taken on a genuine person is properly classified as a genuine sample. As such, this is a metric for the convenience of the spoof detection method as seen by an authorized user. The FAR describes the rate at which a spoof sample is falsely classified as a genuine sample. This rate provides a metric for the degree of security against spoofs provided by the system at a particular operating point. The security and convenience of this spoof detection system trade off in the same way as in the case of biometric matching: a greater TAR can be achieved at the expense of a reduction in spoof detection and vice versa. One possible operating point is where the decision criteria are set to provide a TAR of 99.5% and the resulting overall spoof FAR is approximately

0.9%. Further analysis showed that at this operating point many spoof samples were never accepted as genuine and no single class of spoof had an FAR greater than 15%. This demonstrates that a very strong form of spoof detection can be implemented with an MSI sensor with minimal adverse impact to the genuine user.

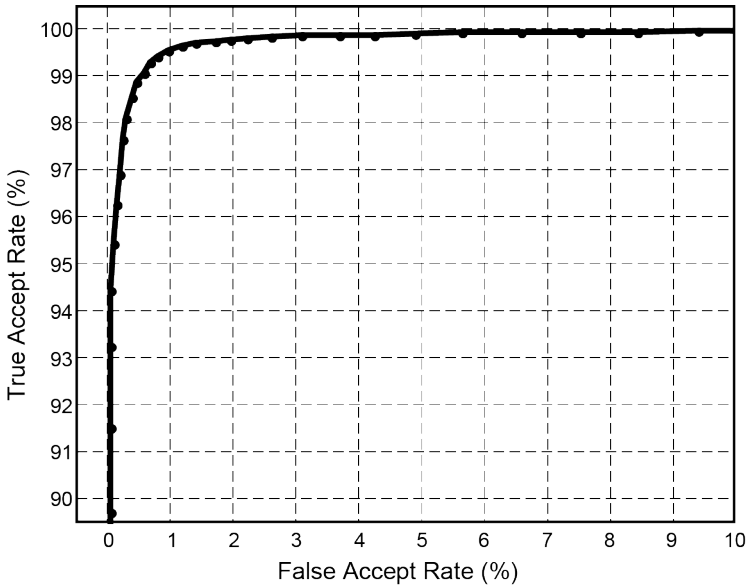

Fig. 10. Error trade-off for multispectral spoof detection.

Summary and Conclusions

The MSI imaging technology acquires multiple, different images of the surface and subsurface characteristics of the finger to provide a secure and reliable means of generating a fingerprint image. Testing performed to date has shown strong advantages of the MSI technology over conventional imaging methods under a variety of circumstances. The source of the MSI advantage is three-fold. First, there are multiple anatomical features below the surface of the skin that have the same pattern as the surface fingerprint and can be imaged by MSI. This means that additional subsurface sources of signal are present for an MSI sensor to gather and compensate for poor quality or missing surface features. Second, the MSI sensor was designed to be able to collect usable biometric data under a broad range of conditions including skin dryness, topical contaminants, poor contact between the finger and sensor, water on the finger and/or platen, and bright ambient lighting. This sensor characteristic enhances the reliability of the MSI sensor and reduces the time and effort required by the authorized user to successfully conduct a biometric transaction. Third, because the MSI sensor does not just measure the fingerprint but instead measures the physiological matrix in which the fingerprint exists, the resulting data provides clear indications of whether the fingerprint is taken from a living finger or some other material. The ability to provide this strong assurance of sample authenticity increases the overall system security and enables the MSI fingerprint sensor to be used in applications and environments in which spoofing is a concern.

Although the MSI imaging technology is a distinctly different means to acquire a fingerprint, testing has demonstrated that the MSI fingerprint is compatible with images collected using other imaging technologies. Such a finding enables the MSI sensor to be incorporated into security systems with other sensors and be used interchangeably. As well, MSI sensors may be deployed in applications in which the new MSI fingerprint images are compared with a legacy database of images collected using different techniques.

Further testing of the MSI sensing technology is underway in both large-scale deployments and a variety of laboratory environments. Results from these tests are certain to add to the body of knowledge regarding the MSI fingerprint technology.

References

Cummins, H. and Midlo, C. (1961) Finger prints, palms and soles. Dover, New York, pp. 38-9.

Derakhshani, R. (1999) Determination of Vitality from a Non-Invasive Biomedical Measurement for Use in Integrated Biometric Devices. Master's Thesis, West Virginia University, http://kitkat.wvu.edu:8080/files/1035/CompleteMain2.PDF.

Duda, R.O., Hart, P.E., and Stork, D.G. (2001) Pattern Classification. John Wiley & Sons, Inc.

Geradts, Z. and Sommer, P. (2006) Forensic Implications of Identity Management Systems. Future of Identity in the Information Society Organization, http://www.fidis.net/fileadmin/fidis/deliverables/fidis-wp6-del6.1.forensic_implications_of_identity_management_systems.pdf.

Hill, P., Canagarajah, N. and Bull, D. Image fusion using complex wavelets, Proc. 13th British Machine Vision Conference, Cardiff, UK, 2002.

Kingsbury, N. Complex wavelets for shift invariant analysis and filtering of signals. Journal of Appl. and Comput. Harmonic Analysis, 10:234–253,2001.

Matsumoto, T., Matsumoto, H., Yamada, K., and Hoshino, S., (2002) Impact of artificial "gummy" fingers on fingerprint systems. Proceedings of SPIE, vol. 4677, http://www.lfca.net/Fingerprint-System-Security-Issues.pdf.

Parthasaradhi, S.T.V. (2003) Comparison of classification methods for perspiration-based liveness algorithm. Master's Thesis, West Virginia University.

Sangiorgi, S. et al. (2004) Microvascularization of the human digit as studies by corrosion casting. J. Anat. 204, pp 123-31.

Shirastsuki, A. et al. (2005) Novel optical fingerprint sensor utilizing optical characteristics of skin tissue under fingerprints. In: Bartels, Bass, de Riese, Gregory, Hirschberg, Katzir, Kollias, Madsen, Malek, McNally-Heintzelman, Tate, Trowers, Wong (Eds.), Photonic Therapeutics and Diagnostics. Proceedings of SPIE vol. 5686, Bellingham, Washington.

Thalheim, L., Krissler, J., and Ziegle, P. (2002) Biometric access protection devices and their programs put to the test. http://www.heise.de/ct/english/02/11/114.